Differentiated radio-over-fiber-based backhauling for dynamic LTE capacity provisioning

Transport différencié basé sur la radio-sur-fibre pour une gestion dynamique de la capacité radio dans les réseaux 4G LTE

Ahmed Haddad
Maurice Gagnaire

2013C002

décembre 2013

Département Informatique et Réseaux
Groupe RMS : Réseaux, Mobilité et Services

Differentiated Radio-over-Fiber-based Backhauling for Dynamic LTE Capacity Provisioning

Ahmed Haddad and Maurice Gagnaire

***Abstract*—It is today widely admitted that existing cellular backhauling needs to be redesigned to cope with radio mobile traffic increase. We have proposed in recent papers an alternative solution called GeRoFAN (Generic Radio-over-Fiber Access Network) exploiting both the benefits of optical transparency and Analog-Radio-over-Fiber (A-RoF). Thanks to A-RoF and reflective modulators used at network terminations, it is possible to mutualize most of the radio equipment at the head of the infrastructure. In this paper, we propose an innovative Control Plane called GeRoFAN-CP aiming at a flexible Radio Frequency (RF) resource allocation according to the time-space fluctuations of the traffic matrix. This control plane relies on two tools. A Quality of Transmission analytical model evaluates the capacity of each cell. A decision support tool defines a set of engineering rules to mitigate the impact of physical layer impairments on this capacity. Supported by the tools mentioned previously, GeRoFAN-CP exploits an iterative algorithm called Differentiated Backhauling Service (DBS) that optimizes the mapping of RFs onto optical channels to achieve a *fluid* management of LTE radio capacity during stable states of the traffic matrix. Numerical results outline that DBS facilitates a more efficient usage of RF resources to the benefit of radio operators.**

***Index Terms*—Quality-of-Transmission (QoT), Radio-over-Fiber (RoF), Long Term Evolution (LTE), Wavelength Division Multiplexing Passive Optical Network (WDM-PON), Mobile Backhauling.**

I. Introduction

The first mile of a fixed or mobile public network represents the highest fraction of the investment and operational costs for an operator due its low level of mutualization [1]. In radio mobile, mobile backhaul refers to the section of carrier's networks that connect Base Transceiver Stations (BTS) to Base Station Controllers (BSC). In existing UMTS 3G mobile networks, BTSs and BSCs referred to Nodes-B and RNCs (Radio Network Controllers) respectively are connected by means of various types of technologies: DSL copper wires, optical fiber pairs or bidirectional line of sight microwave links [2]. Up to these recent years, voice communications have represented the great majority of the traffic transported in radio-mobile networks. In this context, legacy mobile backhaul networks have been based on circuit-oriented T1/E1 connections. It was observed around the year 2000 a regular increase in data traffic in mobile networks through the successive generations of the 3GPP standards known as UMTS, LTE and today LTE-Advanced. These various techniques have enabled the progressive introduction of packet-oriented traffic in mobile backhaul. As an indication, the theoretical peak bit rate per mobile user has evolved from 384 kbps/64 kbps for the downlink/uplink capacities respectively under UMTS in 2003 to 326 Mbps/86 Mbps for the downlink/uplink capacities respectively under LTE in 2010 [3]. Such a growth in capacity imposes a higher cells' density that makes traditional T1/E1 leased lines used as backhaul too expensive to scale up. RoF consists in backhauling radio traffic by means of an optical fiber infrastructure. It can be viewed as a promising technique to facilitate such an evolution by providing a form of mutualization and centralization of the intelligence of the radio system at a remote site. Two variants of RoF are today available: Analog RoF (A-RoF) and Digitized RoF (D-RoF). A-RoF consists in modulating an optical carrier with analog radio signals by using Intensity Modulation Direct Detection (IMDD). D-RoF consists in sampling a modulated radio signal, the obtained digital flow being transported by means of baseband modulated optical carrier. Under A-RoF, several Radio Frequency (RF) signals can be multiplexed within the same optical link using Wavelength-Division Multiplexing (WDM) and Sub-Carrier Multiplexing (SCM). On one hand, the cost-effectiveness of A-RoF with respect to D-RoF has been outlined in [4], where a price ratio ranging between 10 and 15 has been reported. In fact, the current level of technology used for D-RoF circuitry is not scalable to cope with the future traffic increase. On the other hand, several papers have underlined the limited dynamic range of A-RoF [5]. In existing literature, this limitation is mitigated using simple techniques such as uplink radio power control and automatic gain control [4].

In this perspective, we have proposed an alternative network architecture called GeRoFAN (Generic RoF Access Network) based on A-RoF for cellular backhauling [13][11]. One of the original aspects of GeRoFAN access systems is to mitigate the limitations of A-RoF by using an impairment-aware Control Plane (CP) that, unlike the previous techniques, keeps unchanged the radio specifications of the mobile system (power control is a specificity of radio mobile MAC layer). The suitability of two point-to-multipoint backhaul topologies (optical trees and optical loops) for GeRoFAN has been investigated [14][12]. Two main factors justify our preference for WDM trees: they are less sensitive to physical layer impairments than optical loops and optical trees are already under deployment for broadband fixed access. Although the GeRoFAN mobile backhauling can be applied to a mix of Radio Access Technologies (RAT) leveraging on its mutualization opportunities between operators as presented in [15], this paper focuses only on the case of LTE backhauling. More generally, mobile

A. Haddad and M. Gagnaire are with the Networks and Computer Science Department, Institut Telecom - Telecom ParisTech - LTCI - UMR 5141 CNRS. 46, Rue Barrault F 75634 Paris Cedex 13 - France. e-mail: {ahhaddad|maurice.gagnaire}@telecom-paristech.fr.

backhauling evolution is widely debated among equipment vendors and operators. Network survivability, protocol stack, synchronization and packet-oriented mode, energy consumption and traffic offload are among the topics that are discussed. These specific aspects are out of the scope of the present contribution. The main challenge addressed in this paper is the design of an innovative control plane enabling to mitigate the numerous physical layer impairments inherent to A-RoF under dynamic traffic conditions.

This paper is organized as follows. Section II is divided into two sub-sections. The former recalls the main characteristics of the GeRoFAN architecture. The latter underlines A-RoF limitations in the context of GeRoFAN backhauling. Supported by a detailed analytical formulation of the various impairments degrading the Signal-to-Noise (SNR) ratio, we analyze the impact of A-RoF limitations on cellular capacity. A set of rules is proposed as a decision support tool used by GeRoFAN-CP to optimally assign RFs onto OCs. Section III is dedicated to the description of the Differentiated Backhauling Service (DBS) algorithm that is at the basis of the rationale of the GeRoFAN-CP. Exploiting the decision support tool, the DBS algorithm is an iterative optimization aiming at adjusting the Shannon's capacity at each cell according to the current traffic load. In Section IV, we comment simulation results outlining the efficiency of the DBS algorithm in the context of LTE backhauling. Section V concludes the paper.

II. GeRoFAN architecture and RoF limitations

Several hybrid optical-wireless access network architectures have been proposed these last ten years for cellular backhauling ([4], [6], [10]). The specificity of GeRoFAN relies on its capacity to facilitate a high level of mutualization of the backhaul infrastructure and radio resources. The GeRoFAN-CP is MAC-agnostic i.e. it does not impact the MAC protocol of the wireless access system, including radio power control. Thanks to its inherent optical transparency, GeRoFAN may federate different Radio Access Units (RAU) using different RAT such as LTE and WiFi.

A. System Architecture

As illustrated in Figure 1, GeRoFAN access systems can be based on legacy WDM Passive Optical Networks (WDM-PON) already used for fixed broadband access. Several optical trees are connected to the same head-end node referred as the Hybrid Optical Line Termination (HOLT) while an RAU serving a 4G radio cell is connected at the leaf of each optical tree.

The internal architectures of the HOLT and RAUs are detailed in a previous paper [13]. The HOLT concentrates the great majority of the intelligence of the system. It is in charge of the management of a pool of OCs and a pool of RFs that can be used for upstream/downstream traffic. By managing an RF-onto-OCs mapping matrix at the HOLT, the GeRoFAN-CP determines which RFs have to be assigned to which OCs in order to satisfy optimally the required bandwidth at each radio cell. The HOLT is equipped with a set of optical transceivers including Tunable Laser Diodes (T-LD) for

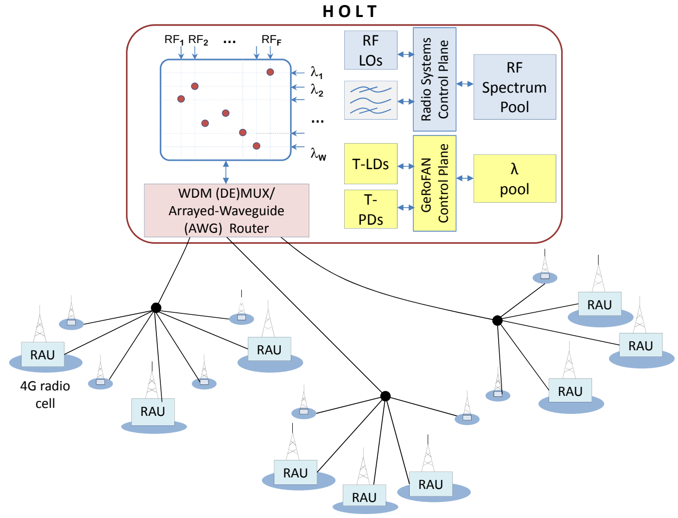

Fig. 1: The GeRoFAN multi-tree architecture and structure of the HOLT.

optical signal transmissions and Tunable Photo-Detectors (T-PD) for optical signals reception. During stable traffic periods, the set of OCs modulated with specific RFs at the HOLT is multiplexed via a WDM multiplexer (MUX). A low-cost Arrayed Wave Guide (AWG) Router broadcasts each OC to its designated optical tree. An RAU is equipped with a Reflective Absorption Modulator (RAM) integrated with Semiconductor Optical Amplifiers (SOA) and a Fiber Bragg Grating based Reconfigurable Optical Add/Drop Multiplexer (FBG-based ROADM). Being dynamically informed by the HOLT via an out-of-band signaling channel λ_s, each RAU knows which downstream OC it has to extract from the received WDM multiplex. For downstream radio traffic, the RFs are extracted, amplified and radiated in the considered cell. For upstream radio traffic, a continuous-wave OC generated at the HOLT is extracted at the RAU to be SCM-modulated by the aggregated radio signal received from all mobile users located at the considered cell. Once this SCM-modulated OC comes back to the HOLT, it is isolated first by means of an FBG-based demultiplexer (DEMUX) and demodulated by a T-PD. In other terms, the GeRoFAN-CP manages a logical RF-onto-OC switching matrix while respecting the cellular planning rules of the radio system. At the RAU, the reconfiguration of the ROADM to extract the right OC and the setting of the bias voltage to drive the RAM are carried out from the signaling information transported by λ_s. Upstream signaling information are sent by RAUs in TDMA-mode. Thanks to the centralization at the HOLT, GeRoFAN acquires a global view of the traffic load evolution over the set of cells served by the optical trees. To outline the benefit of the GeRoFAN-CP, let us consider that the three optical trees illustrated in the Figure 1 cover a leisure, a business and a housing areas respectively. In such a configuration, the GeRoFAN-CP aims at coping with time and space fluctuations of the traffic matrix. Indeed, traffic peaks occur at different time periods of the day depending on the area. Instead of dimensioning radio resources on the basis of the peak load, the GeRoFAN-CP exploits a form of macroscopic statistical multiplexing in the assignment of radio resources at a multi-cell scale [8]. Unlike our previous publications that were focused on static traffic scenarios, we consider in this paper the case of dynamic traffic.

B. RoF transmission limitations

As mentioned in our introduction, A-RoF signals propagation is subject to physical layer impairments that degrade the SNR of the radio channel at each RAU. The Shannon's capacity within each cell depends on RoF signal quality after its propagation through the GeRoFAN system. The main originality of our work consists in analyzing and quantifying the origin and the amplitude of each noise. Thanks to a deep knowledge of these parameters, we determine the best suited RF-onto-OC mapping strategy enabling to satisfy during each stable traffic period the upstream traffic load. In a dynamic traffic context, where all radio cells are not subject to the same load, our main challenge consists in determining the *optimal* SNR at each cell that adjusts the Shannon's capacity to the requested bandwidth in the cell. This means that too high SNRs, thus leading to a higher Shannon's capacity than required, have to be prevented if they are achieved at the detriment of insufficient SNRs at other radio cells subject to a high traffic load. To assess the impact of the various RoF impairments on the SNR of an RF channel, we have developed a comprehensive analytical model called Quality of Transmission tool (or QoT-tool) that packages all noises inherent to the GeRoFAN system. Table I summarizes the analytical expressions of these noises. Considered noises are:

- The Modulation Penalty (MP) is expressed as the noise figure F of the RoF link that depends on the RF gain G of the RAM. Figure 2 illustrates the evolution of F and G with respect to the OC wavelength.
- Intermodulation Distortions (IMDs) include IMD-RAM, due to the non-linearity of the reflective modulator, IMD-OFDM due the multi-subcarrier nature of the LTE radio signal, and Optical Beat Interference (OBI) due to the coupling effects between upstream OCs at the receiver. Figure 3 illustrates the IMD-RAM SNR penalty according to the number of RF channels per OC.
- Rayleigh Back-Scattering (RBS) noise is inherent to reflective systems as GeRoFAN. We depict the evolution of the RBS SNR penalty with fiber length in Figure 4.
- The QoT-tool also considers both linear and non-linear impairments usually considered in fiber-based analog communication systems as Chromatic Dispersion (CD), Polarization Mode Dispersion (PMD) and fiber Non-Linear Effects (NLEs). The main considered NLEs are Stimulated Raman Scattering and Four-Wave Mixing. They are formulated as in [24]. The QoT-tool also includes heterodyne crosstalk (XT) and homodyne crosstalk whose penalty is modeled as in [25]. These optical crosstalks occur at the AWG router, the MUX/DEMUX device and the ROADM. Figure 5 shows the evolution of CD penalty with the number of RFs per OC for 10 Km propagation.
- Miscellaneous system penalties, including SOA spontaneous emissions noise and splitter loss are also considered in the QoT-tool.

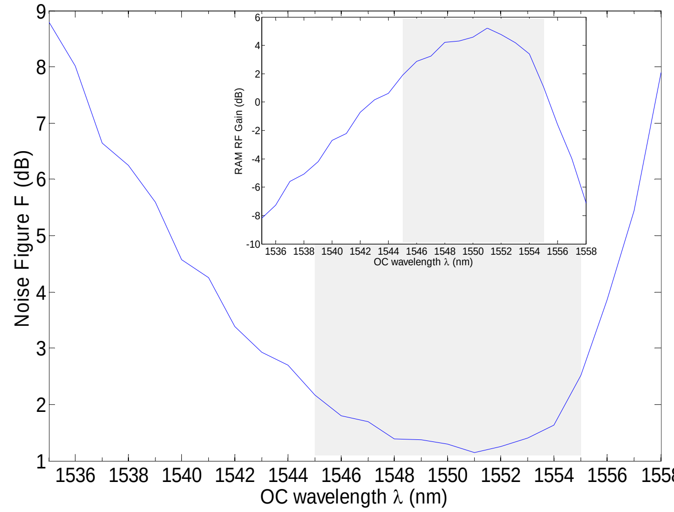

Fig. 2: Noise Figure F of the modulator *vs.* OC wavelength at $10mW$ laser output optical signal power. Inset: Modulator RF Gain. Dashed grey area indicates the OCs with low MP penalty (higher RF Gain).

Based on RoF impairment analytical formulations in Table I, we derive the relevant factors that contribute to noise amplitude. Apart the length of the optical link that cannot be changed once the GeRoFAN network is deployed, these factors constitute the action levers the GeRoFAN-CP exploits to mitigate the impact of each impairment. The action levers are: the wavelength value of the OC $[\lambda]$, its rank within other propagating OCs in the fiber $\lambda_{i|1...W}$, the total number of RFs F, the value of the microwave frequency $[f]$, its rank among the other RF channels transported by the same OC $f_{i|1...F}$.

From the analytical modeling of each impairment, we get the behavior of its amplitude with respect to its associated action levers. This enables to derive rules $\mathcal{R}_\ell$ in order to manage the SNR penalty of each impairment. To quantify the degree of compliance of an OC λ to a given rule $\mathcal{R}_\ell$, we compute its rank $r_{\mathcal{R}_\ell}(\lambda)$. A rank $r_{\mathcal{R}_\ell}$ of an OC is a non-negative real function from the λ-pool $\{\lambda_1, \ldots, \lambda_W\}$ into $[0, 1]$ designed such that the higher the value of the rank, the higher the compliance of that OC to the rule $\mathcal{R}_\ell$.

The set of rules $\mathcal{R}_\ell$ of each impairment $\mathcal{I}$ and their associated rank equations $r_{\mathcal{R}_\ell}$ are detailed in Table II. They constitute a decision support tool used by the GeRoFAN-CP to investigate the optimal RF backhauling solution.

III. DIFFERENTIATED BACKHAULING SERVICE (DBS) ALGORITHM

As aforementioned, thanks to RoF, GeRoFAN-CP acquires at the HOLT a global view of the system dynamics (traffic load distribution). The CP keeps a steady monitoring of the evolution of the aggregated traffic load at each cell in the network. Upon the observation reported by the traffic load manager, the CP activates the Differentiated Backhauling Service (DBS) algorithm as illustrated in Figure 6. The DBS algorithm relies on an iterative procedure aiming to adjust the Shannon's capacity within each cell according to its traffic

TABLE I: Mathematical expressions used in our A-RoF analytical model.

MP	Although the RAM performs an amplification of the optical signal (via the SOA), the modulation efficiency of an RF channel may be degraded due to the intrinsic noise of the modulator and the noise of the modulating radio signal. The modulation penalty depends on the SNR of both (modulating) radio signal and optical carrier at the input of the RAM. The modulation penalty is computed as the noise figure F of the RoF modulator: $$F = \frac{N_{out}}{k \cdot T \cdot B \cdot G} \quad (1)$$ N_{out}: the noise power at the output of the RAM; k: The Boltzmann's constant; T: the temperature; B: the noise bandwidth; $G = \lvert \frac{P_{out}}{P_{in}} \rvert$: the RF link gain defined as the ratio of the microwave power at the output of the photo-detector with respect to the RF power at the input of the RAM. The analytical expression of the RF link gain is reported in [16].
IMD-RAM	Because of the non-linearity of the RAM transfer function f [17], third order intermodulation (IMD3) products that arise from mixing between several RFs may fall inside the band of an designated operational RF channel, thus degrading its SNR. Using a Taylor expansion of f under a low-amplitude signal assumption, the IMD3 optical noise generated by 2 tones (i,j) (resp. 3 tones (i,j,k)) that falls at RF $l = 2i \pm j$ (resp. $l = i \pm j \mp k$) is computed according to Equation 2a (resp. 2b): $$N_{2i\pm j} = \frac{3}{4} \cdot \frac{K_3}{3!} \cdot V_b^3 \cdot m_i^2 m_j \cdot P_o \quad (2a)$$ $$N_{i\pm j\mp k} = \frac{3}{2} \cdot \frac{K_3}{3!} \cdot V_b^3 \cdot m_i m_j m_k \cdot P_o \quad (2b)$$ m_i: Optical Modulation Index (OMI) of RF channel i; V_b: DC bias voltage of the RAM; $K_3 = \frac{\mathrm{d}^3 f}{\mathrm{d}V^3}\rvert_{V=V_b}$: 3^{rd} order RAM non-linearity parameter computed as the 3^{rd} derivative of f with respect to the voltage V at V_b; P_o: Average received optical power.
IMD-OFDM	For a RF OFDM-modulated channel, such as in LTE or WiMAX, the non-linearity of the modulator generates IMD noises due to beating between OFDM Subcarriers (SCs). The analytical study in [18] shows that distortions spread out over a bandwidth three times larger than the RF bandwidth thus penalizing the SNR of the RF channel itself and its adjacent (left and right) neighbors. The detected intensity of third order IMDs falling at RF channel ℓ is [18]: $$I(\ell) = \frac{1}{6} d_{\ell-1}^2 + \frac{2}{3} d_\ell^2 + \frac{1}{6} d_{\ell+1}^2 \quad (3)$$ $d_i^2 = \frac{(P_o K_3 m_o^2 V_b^3)^2}{2} \cdot \mathcal{M}(N)$: The relative amplitude of IMD noises created by OFDM SCs composing the RF channel i; m_o: OMI of single OFDM SC; $\mathcal{M}(N)$: total number of IMD3 composite products produced by the beating of N equally-spaced OFDM SCs computed as in [19].
OBI	In a WDM-PON system, two upstream OCs with the same wavelength may be modulated by distinct radio signals at RFs i and j, then combined at the optical coupler and detected. Because of the square-law of the detection process, the beating between the OCs generates IMD-like interference between their subcarrier RF channels that may fall on a designated RF channel $\ell = 2i \pm j$. The frequency spectrum of the interference term is determined by convolving the frequency spectra of the OCs. The Power Spectral Density (PSD) of the OC at the output of the DFB laser is approximated by a Lorentzian function with a line-width broadened by the frequency chirp of the RAM. Following the development in [20], we express the Signal to Interference Ratio (SIR) defined as the ratio of the signal power to the OBI noise power falling within the bandwidth of RF channel ℓ as: $$SIR = \frac{\frac{1}{2}\langle m_\ell^2 P_{o,\ell}^2 \rangle}{\int_{B_\ell} N_{ij}(f)\,\mathrm{d}f} \quad (4)$$ where the PSD of the OBI noise due to the beating of OCs i and j is: $$N_{ij}(f) = 4\sqrt{P_{o,i}P_{o,j}}\sqrt{f(V_i)f(V_j)}(S_i(f) \otimes S_j(f)) \cdot \langle \cos^2 \theta_{ij} \rangle \quad (5)$$ m_ℓ: the OMI of RF channel ℓ; B_ℓ: the bandwidth of RF channel ℓ; $S_k(f)$: The Lorentzian PSD of the electric field of OC modulated by RF k. $P_{o,k}$: Received optical power of OC modulated by RF k; θ_{ij}: the difference in polarization angle between fields i and j; $\otimes$: Convolution operator; $\langle \cdot \rangle$: Time average operator.
RBS	In reflective network systems like GeRoFAN, noise due to interference of the reflected modulated optical wave with Rayleigh back-scattered incident wave degrades the receiver sensitivity. To assess the impact of RBS, we follow the analytical approach in [21]. PSD of RBS noise evaluated along an optical link of length L is: $$N(f) = \frac{10R_{rb}^2(2\alpha L + e^{-2\alpha L} - 1)}{9} \cdot (S(f) \otimes S(f)) \quad (6)$$ $S(f)$: PSD of the optical signal at the output of the laser, assumed as a Lorentzian distribution; α: Fiber attenuation coefficient; R_{rb}: RBS reflectance of the fiber.
CD	Thanks to its simplicity, GeRoFAN uses double side-bands modulation to modulate the optical carrier. However, because of CD, the OC, its sidebands, as well as their carried RF channels, propagate at different velocities. At the photo-detector, when beating the two sidebands of the optical channel to extract the radio signals, a power fading at each RF channel is reported due to their velocity mismatch [22]. After transmission over optical fiber of length L and CD coefficient D at OC λ, CD penalty is measured in terms of average squared Error Vector Magnitude (EVM): $$\langle EVM^2 \rangle \simeq \frac{[(N+1) + \sum_{-N/2}^{N/2} \eta^2 \cos(\frac{\omega_n^2}{2} - \frac{\lambda^2 DL}{2\pi c})^2 - 2\eta \exp(\frac{-\sigma^2}{2}) \sum_{-N/2}^{N/2} \cos(\frac{\omega_n^2}{2} - \frac{\lambda^2 DL}{2\pi c})]}{N} \quad (7)$$ $\eta = \lvert \frac{J_1(m)}{J_o(m)} \rvert$: the relative amplitude of the optical carrier to its first-order side-bands; J_i: first kind Bessel function of order i; m: OMI of the total SCM RF signal modulating the OC; N: Number of OFDM SCs of a RF channel; ω_n: angular frequency of the n^{th} OFDM SC; σ: Average RF phase noise power.
PMD	At the receiver, the RF signal is extracted from its OC by the heterodyne beating between the carrier and its SCs. Because of PMD, the polarizations of the OC and its RFs become misaligned which causes fading of the RF power after detection. The SNR power penalty caused by PMD at microwave frequency f accumulated over an optical link of length L is [24]: $$\delta = \cos(\pi \cdot f \cdot \tau) \quad (8)$$ $\tau = \beta\sqrt{L}$: the differential group delay of the fiber; β: PMD coefficient of the fiber.
Heterodyne XT	When demultiplexing WDM signals, crosstalk (XT) arises from coherent mixing of the received OC with a crosstalk wave on the PD, originating a beat noise locally at the receiver. At the output of the DEMUX, the heterodyne XT is induced between the extracted OC and the leakage of remaining OCs. Assuming a uniform spectral response of the FBG, the Inter-Channel Crosstalk (ICCT) in the i^{th} OC due to the j^{th} OC is [23]: $$ICCT_{j/i} = \frac{\int \lvert H_i(\omega) S_j(\omega - j \cdot \omega_o) \rvert^2 \mathrm{d}\omega}{\int \lvert H_i(\omega) S_i(\omega) \rvert^2 \mathrm{d}\omega} \quad (9)$$ $H_k(\omega)$: The FBG spectral response of the k^{th} OC; $S_k(\omega)$: The modulation spectrum of the k^{th} OC; ω_o: the WDM channel spacing.

TABLE II: Action levers of each impairment $\mathcal{I}$ and rules $\mathcal{R}_\ell$ to mitigate its impact.

$\mathcal{I}$	Levers	Rules $\mathcal{R}_\ell$ to mitigate the impairment $\mathcal{I}$ and rank equations
MP	$[\lambda]$	$\mathcal{R}_1$: **Select the middle-right OCs of the λ-pool.** For a λ-pool with size W OCs, the rank of an OC with index k is: $r(\lambda_k) = \left(\frac{W}{2} - k\right)^{-2}$ if $k < \lfloor W/2 \rfloor$ and $r(\lambda_k) = \left(k - \frac{W}{2} + 1\right)^{-1}$ otherwise, where $\lfloor x \rfloor$ denotes the integer floor of x.
IMDs	$[\lambda]$	$\mathcal{R}_1$: **Select the outside-right position OCs of the λ-pool, i.e. long wavelengths.** For a λ-pool with size W OCs, the rank of an OC with index k is: $r(\lambda_k) = \left(\frac{W}{2} - k\right)^{-2}$ if $k < \lfloor W/2 \rfloor$ and $r(\lambda_k) = (W - k + 1)^{-1}$ otherwise, where $\lfloor x \rfloor$ denotes the integer floor of x.
	$f_{i\vert 1..F}$	$\mathcal{R}_2$: **IMD-free RF mapping.** To achieve IMD-free RF mapping, radio channels are placed according to position marks specified by the Golomb Ruler as in [9]. Assuming $\mathcal{P}_{f_i \in \lambda_k}$ the number of IMD3 products within λ_k and falling on RF f_i, δ_i^k a binary variable equals to 1 if f_i modulates λ_k and 0 otherwise, then: $r(\lambda_k) = 1 - \frac{\sum_{i=1}^{F} \delta_i^k \cdot \mathcal{P}_{f_i \in \lambda_k}}{1 + \sum_{i=1}^{F} \sum_{\ell=1}^{W} \delta_i^\ell \cdot \mathcal{P}_{f_i \in \lambda_\ell}}$
		$\mathcal{R}_3$: **Two neighboring RFs should not be carried by the same OC (Mitigates IMD-OFDM).** Since the maximum number of overlapping noises in an OC due to IMD-OFDM is equal to $2(F-1)$, the rank of an OC with index k is: $r(\lambda_k) = 1 - \frac{\sum_{i=1}^{F} \delta_i^k \cdot (\delta_{i-1}^k + \delta_{i+1}^k)}{2(F-1) + 1}$
	F	$\mathcal{R}_4$: **Minimize the number of RF carried by an OC.** $r(\lambda_k) = 1 - \frac{\mathcal{F}(\lambda_k)}{F+1}$, where: $\mathcal{F}(\lambda_k)$ the number of RFs carried by λ_k and F the total number of distinct RFs in the cellular system.
RBS	$[\lambda]$	$\mathcal{R}_1$: **Select outside (right or left) position OCs of the λ-pool, i.e. long or short wavelengths.** For a λ-pool with size W OCs, the rank of an OC with index k is: $r(\lambda_k) = \frac{\frac{W}{2} - k}{\frac{W}{2} - 1}$ if $k \leq \lfloor W/2 \rfloor$ and $r(\lambda_k) = \frac{2(k - \frac{W}{2})}{W}$ otherwise, where $\lfloor x \rfloor$ denotes the integer floor of x.
CD	$[\lambda]$	$\mathcal{R}_1$: **The lower the OC wavelength, the lower the CD penalty.** The rank of an OC with index k in the λ-pool of size W is: $r(\lambda_k) = \frac{W+1-k}{W}$
	F	$\mathcal{R}_2$: **Minimize the number of RFs carried by an OC.** $r(\lambda_k) = 1 - \frac{\mathcal{F}(\lambda_k)}{F+1}$, where: $\mathcal{F}(\lambda_k)$ the number of RFs carried by λ_k and F the total number of distinct RFs in the system.
XT, NLEs	$\lambda_{i\vert 1..W}$	$\mathcal{R}_1$: **Increase the channel spacing between OCs that modulate the same RF (Mitigates both XT and NLEs).** Defining $\mathcal{I}_{i,k} = \{\ell \in \{1..W\} \backslash \{k\}; f_i \in \lambda_\ell\}$: the index of all OCs, except λ_k, that carry RF f_i. The rank of an OC λ_k is: $r(\lambda_k) = 1 - \frac{\sum_{i=1}^{F} \sum_{\ell \in \mathcal{I}_{i,k}} \frac{\delta_i^k}{\lvert k-\ell \rvert}}{\sum_{j=1}^{W} \sum_{i=1}^{F} \sum_{\ell \in \mathcal{I}_{i,j}} \frac{\delta_i^j}{\lvert j-\ell \rvert}}$
		$\mathcal{R}_2$: **Select long wavelength OCs (Mitigates SRS).** The rank of an OC λ_k is: $r(\lambda_k) = \frac{k}{W}$.
		$\mathcal{R}_3$: **Select FWM-free OCs (Mitigates FWM).** To achieve FWM-free OCs, optical channels are selected according to position marks specified by the Golomb Ruler as in [9]. Assuming $\mathcal{P}_{k \in 1..W}$ the number of FWM tones generated due to the presence of λ_k in the pool $\{\lambda_1..\lambda_W\}$, then: $r(\lambda_k) = 1 - \frac{\mathcal{P}_{k \in 1..W}}{1 + \sum_{\ell=1}^{W} \mathcal{P}_{\ell \in 1..W}}$.

Nota: The terminology "middle-right", "outside-right/left" OCs mentioned for MP, IMDs and RBS rules refer to the range of the most efficient OCs in the C-band to mitigate the effect of these impairments. These ranges have been determined empirically from Figures 2, 3 and 4 where they are identified by grey dashed areas. For instance in Figure 3, "outside-right" OCs correspond to the range $[1545\ nm, 1565\ nm]$.

load. Two variants of the DBS algorithm, namely DBS$^-$ and DBS$^+$, are executed by the CP in case of traffic decrease or increase respectively.

If both a traffic load increase and decrease are observed at the same time in two different cells respectively, the CP averages both magnitudes and decides accordingly to launch the appropriate variant of the DBS. Once DBS achieves the optimal RF-onto-OCs mapping solution, reconfiguration information are encoded into the signaling OC λ_s and broadcasted to each RAU.

Assuming $\zeta = \{C_k, 1 \leq k \leq |\zeta|\}$ the set of radio cells, $F = \{f_i, 1 \leq i \leq |F|\}$ the set of distinct RFs used in the cellular planning and $\Lambda = \{\lambda_j, 1 \leq j \leq p\}$ the set of required OCs, the DBS algorithm investigates the optimal RF-onto-OCs placement solution by modifying the $|F| \times p$ matrix $S^{(p)}$ defined as: $S_{ij}^{(p)} = C_k$ meaning that RF f_i assigned to cell C_k is carried by OC λ_j. By convention, $S_{ij}^{(p)} = 0$ means that there is no cell served by RF f_i transported by OC λ_j. It has to be noted that if multiple RFs are assigned to the same cell C_k, the value C_k appears several times on the same column of $S^{(p)}$. Since the RF-onto-OCs remapping has to keep unchanged the cellular RF planning, the modification of $S^{(p)}$ is achieved by circular shift along the same row of the matrix (i.e., by permutating $S_{ij}^{(p)}$ and $S_{i\ell}^{(p)}$). To evaluate the impact of the new placement on the capacity provided to each cell, we define similarly to $S^{(p)}$, the $|F| \times p$ matrix ρ. Element ρ_{ij} expresses the ratio of the gap between the offered and the

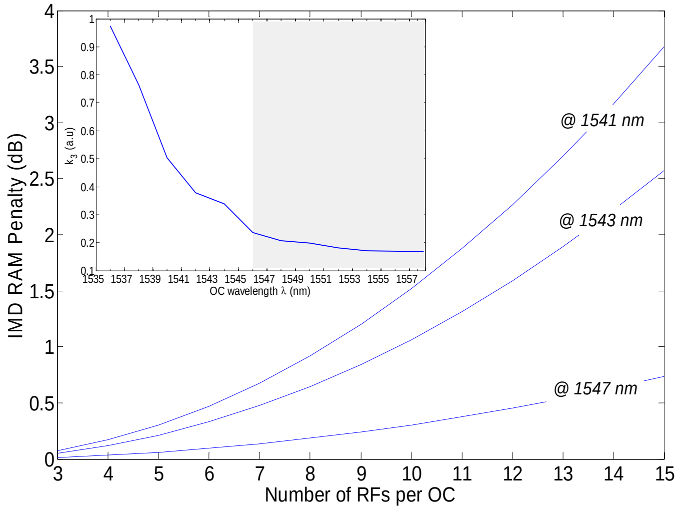

Fig. 3: IMD penalty *vs.* the number of RFs per OC at different wavelength channels assuming an equally spaced RF mapping. Inset: 3^{rd} order RAM non-linearity parameter (k_3). Colored grey area indicates the range of OCs with low IMD penalty.

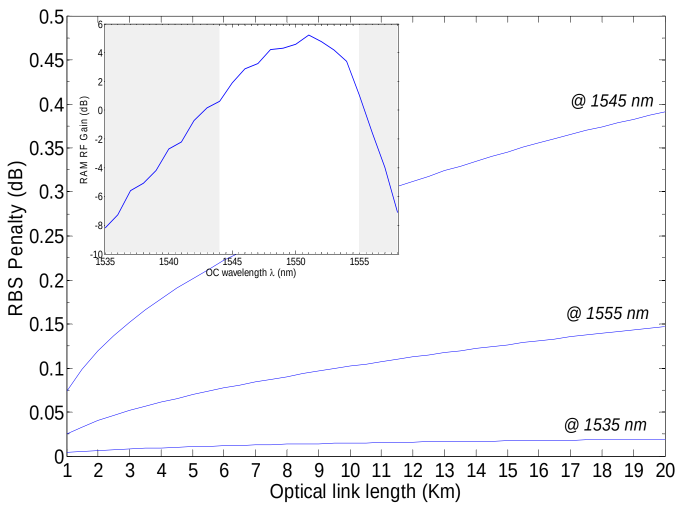

Fig. 4: RBS penalty *vs.* the RAU-HOLT distance at different wavelength channels. Inset: RAM RF Gain. Colored grey area indicates the range of OCs with low RBS penalty.

required capacities normalized to the required capacity at cell $S_{ij}^{(p)} = C_k$. In consequence, $\rho_{ij} > 0$ indicates an excess in the offered capacity, while $\rho_{ij} < 0$ means that only a fraction of the offered load is provisioned.

A. *DBS at traffic load increase (DBS^+):*

The CP runs the DBS$^+$ algorithm when an increase of the traffic load is reported by the traffic monitor. DBS$^+$ provides hot-spot cells with the needed radio capacity by remapping RFs-onto-OCs while requesting from the λ-broker, the lowest additional number of required OCs. The algorithm takes in input the traffic load distribution among cells and the best RF-onto-OCs mapping solution $S^{(p)^*}$ achieved with p OCs. Considering $\zeta^{\uparrow}$ the set of cells experiencing an increase of the traffic load, then the quality of a given solution $S^{(p)}$ is

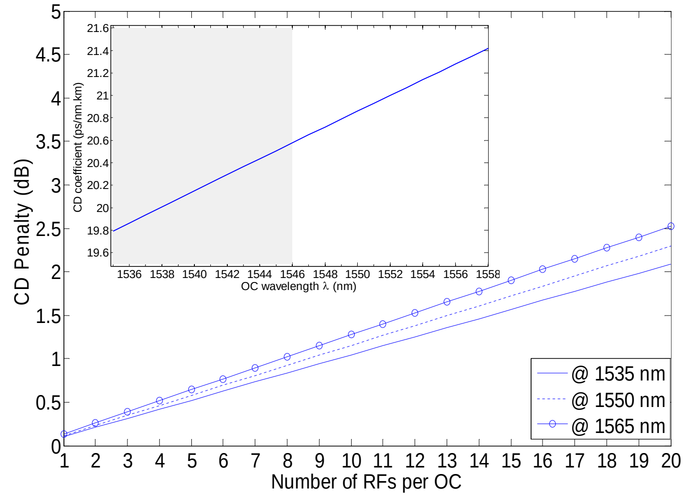

Fig. 5: CD penalty *vs.* the number of RFs per OC with 10 Km fiber length. Inset: CD coefficient (D) *vs* OC wavelength. Colored grey area indicates the range of OC with low CD penalty.

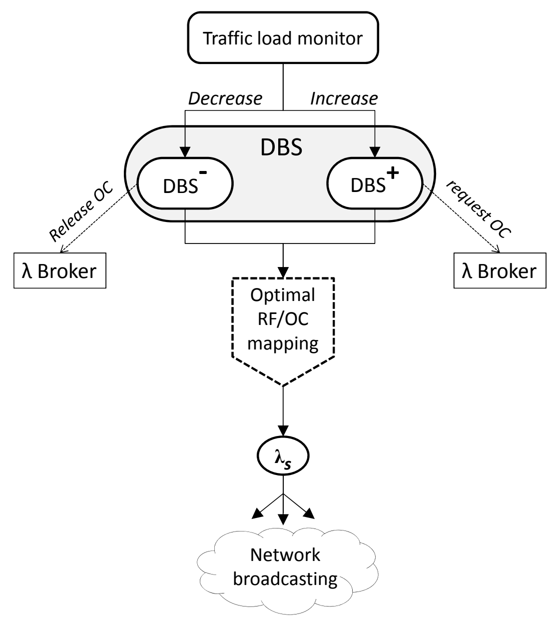

Fig. 6: DBS activation by the GeRoFAN-CP and interaction with the λ-broker.

evaluated using the quadratic mean Ω of the radio capacity computed as in Equation 10:

$$\Omega = \frac{\sqrt{\sum_{(i,j);S_{ij}^{(p)} \in \zeta^{\uparrow}} \rho_{ij}^2}}{|\zeta^{\uparrow}|} \tag{10}$$

The lower the value of Ω, the better is the RF-onto-OCs mapping solution. The use of the quadratic mean in Equation 10 instead of a simple average makes the minimization of Ω yielded by the minimization of all its elements $|\rho_{ij}|$.

As depicted in the flowchart of Figure 10, DBS$^+$ investigates the best mapping solution that can be achieved with at most p OCs. For that sake, it calls two main algorithmic blocks namely the Blind Search Box (BSB) and the Guided Search Box (GSB) whose detailed working is described respectively in subsections III-C and III-D. Unless BSB or GSB triggers an exit, the quality of solutions $S^{(p-1)^*}$ and $S^{(p)^*}$ are compared, making DTS$^-$ either to carry out a new iteration with an additional OC or to exit with $S^{(p-1)^*}$.

B. DBS at traffic load decrease (DBS^-):

When a decrease of the traffic load is reported in some cells, a capacity excess is likely to occur in that cells. The CP runs the DBS$^-$ algorithm which targets to pack RFs more closely together into the minimum number of OCs. Hence, freshly vacant OCs can be released and given back to the λ-broker (c.f. Figure 6). However, because a dense packing of RFs into OCs is likely to increase the beating between RFs and thus to degrade their radio capacities, DBS$^-$ carries out the RF packing process iteratively over all used OCs. By doing so, the algorithm ensures that only the most *least penalizing* OCs are released. We call *least penalizing* OCs, those whose their release makes the induced capacity loss remains fulfilled by the capacity excess due to the load decrease. To check the quality Ω of a given solution $S^{(p)}$, DBS$^-$ uses Equation 11 which not only focuses on $\zeta^{\downarrow}$, the set of under-loaded cells, but also includes cells of set $\widetilde{\zeta} = \{S^{(p)_{ij}} \in \zeta; \rho_{ij} < 0\}$ which experience a need in capacity subsequent to the RF packing:

$$\Omega = \frac{\sqrt{\sum_{(i,j);S^{(p)_{ij}} \in \zeta^{\downarrow} \bigcup \widetilde{\zeta}} \rho_{ij}^2}}{|\zeta^{\downarrow}| + |\widetilde{\zeta}|} \tag{11}$$

The flowchart of DBS$^-$ is depicted in Figure 9. Similarly to DBS$^+$, DBS$^-$ calls the BSB and GSB blocks to search for the best RF-onto-OC mapping. To identify the *least penalizing* OC $\widetilde{\lambda}$ that should be released, the algorithm runs a Tabu-search among all OCs using a Tabu list $\mathcal{Z}$. The release of $\widetilde{\lambda}$ is made effective when the quality of the solution $S^{(p-1)^*}$ (which doesn't require $\widetilde{\lambda}$) is at least equal to the solution $S^{(p)^*}$ (which uses $\widetilde{\lambda}$). Unless BSB or GSB triggers an exit, the algorithm stops either when the Tabu list becomes full or the theoretical lower bound of required number of OCs is achieved.

C. The Blind-Seach Box (BSB)

The DBS algorithm relies on the BSB algorithmic block whose flowchart is illustrated in Figure 8. The rationale of the BSB is to feed cells that need capacity (i.e. cells with $\rho_{ij} < 0$) with the capacity excess observed in under-loaded cells (i.e. cells with $\rho_{ij} > 0$). BSB adjusts the radio capacity to the load level by permutating OCs transporting under-loaded RFs with OCs carrying overloaded RFs.

BSB starts an iteration t by identifying the cell whose RF i should be relocated from its OC j to another OC $j^\star$. If DBS$^+$ is applied, the targeted cell is $S^{(p)}{}_{ij} = \{S^{(p)}{}_{k\ell} \in \zeta^{\uparrow}; \max_{k\ell} |\rho_{k\ell}|\}$, while for DBS$^-$ it would be $S^{(p)}{}_{ij} = \{S^{(p)}{}_{k\ell} \in \zeta^{\downarrow} \bigcup \widetilde{\zeta}; \max_{k\ell} |\rho_{k\ell}|\}$.

$$r(\lambda_k) = \begin{cases} |\rho_{ij} - \rho ik| & \text{if } S^{(p)_{ik}} \neq 0 \\ \\ \max_{\ell=1..|\Lambda|} r(\lambda_\ell) & \text{if } S^{(p)_{ik}} = 0 \end{cases} \tag{12}$$

To find OC $j^\star$, BSB ranks all OCs according to Equation 12. After rank normalization, BSB checks whether the rank of the OC $j^\star_{t-1}$, i.e. the OC selected at the previous iteration $t-1$, equals to $\max_{k=1..|\Lambda|} r(\lambda_k)$. In that case, ranks are updated as in Equation 13 to prevent the OC $j^\star_{t-1}$ from being selected at the current iteration t, however if $r(\lambda_{j^\star_{t-1}}) < \max_{k=1..|\Lambda|} r(\lambda_k)$ then there is no need for BSB to update the ranks.

$$\begin{cases} r(\lambda_k) = r(\lambda_k) + \dfrac{r(\lambda_{j^\star_{t-1}})}{2(|\Lambda| - 2)} \\ r(\lambda_{j^\star_{t-1}}) = \dfrac{r(\lambda_{j^\star_{t-1}})}{2} \end{cases} \tag{13}$$

Equation 13 penalizes the rank of OC $j^\star_{t-1}$ by dividing it by 2 at the profit of the other OCs (except the original OC j).

We evaluate the capacity matrix ρ of the new RF-onto-OCs mapping solution obtained by relocating RF i from OC j to the OC $j^\star$ with the highest rank. Using Equation 10 (respectively Equation 11) if DBS$^+$ (respectively if DBS$^-$) is applied, quality Ω of the new mapping solution is compared with the best quality achieved Ω^*. The BSB algorithm is iterated once again, however, it can lead to an exit if Ω^* achieves a threshold value Ω^{th}, or it moves to the GSB block if a local counter α attains a threshold value α^{th}.

The scenario depicted in Figure 11 illustrates the working principle of BSB. Let's consider a network of 10 cells using 3 distinct RFs mapped onto 4 OCs as illustrated by matrix $S^{(4)}$. Let's assume that BSB is called during the execution of DBS$^+$ algorithm, the former identifies RF f_1 assigned to cell 1 as the RF to relocate from its OC λ_1. The 4 used OCs are ranked according to Equation 12. Since OC λ_3 has been selected as OC $j^\star$ at the previous iteration, BSB updates the ranks according to Equation 13. The updated ranking enables OC λ_4 to be selected for RF permutation with OC λ_1. With the new RF-onto-OC mapping solution, BSB exploits the QoT-tool to compute its capacity matrix ρ and to evaluate its quality according to Equation 10.

D. The Guided-Seach Box (GSB)

The flowchart of the GSB algorithm is presented in Figure 7. GSB identifies the RF i to relocate similarly to BSB. Nevertheless, unlike BSB, the GSB algorithm relocates RF i from its OC j to a new OC $j^\star$ using a guided optimization approach. In fact, supported by the QoT-tool, GSB quantifies the share of each impairment in the total SNR penalty of RF i in order to identify the most penalizing impairment $\mathcal{I}$ responsible for such a capacity degradation. Using the rules $\mathcal{R}_\ell$ recommended to manage the impairment $\mathcal{I}$ in Table II, GSB computes the rank $r_{\mathcal{R}_\ell}(\lambda_k)$ of each OC $k \neq j$. Note that the rank of an OC k is computed after assuming an RF permutation between OC k and OC j. To prevent the selection of the same OC j, we set $r_{\mathcal{R}_\ell}(\lambda_j) = 0$. When $\mathcal{L}$ rules are

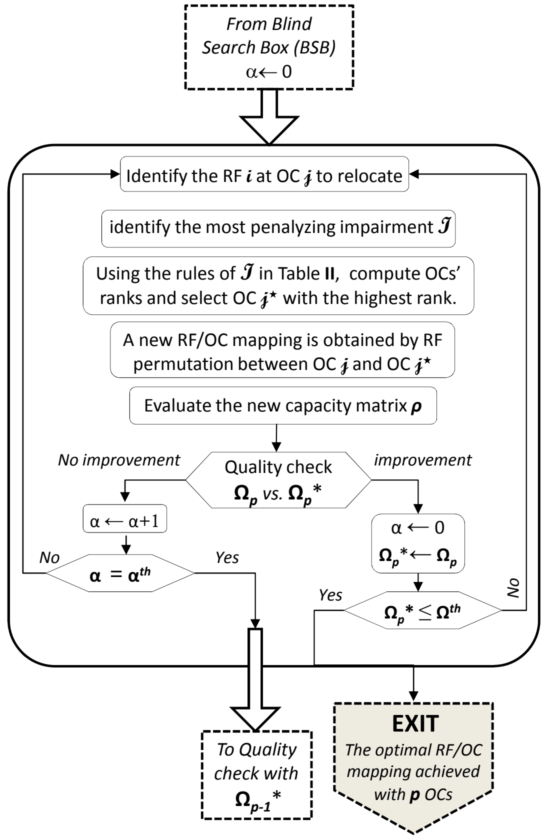

Fig. 7: Guided Search Box (GSB) flowchart.

involved for impairment $\mathcal{I}$, we compute the aggregated rank $r(\lambda_k)$ of an OC k as in Equation 14. Once the highest ranked OC has been selected as the OC $j^{\star}$, the algorithm is continued similarly to BSB.

$$r(\lambda_k) = \prod_{\ell=1}^{\mathcal{L}} r_{\mathcal{R}_\ell}(\lambda_k) \tag{14}$$

To illustrate the main steps of the GSB algorithm, let's consider again the previous case of a 10-cells network using 3 distinct RFs mapped onto 4 OCs from a λ-pool of $W = 24$ OCs. As depicted in Figure 11, GSB identifies RF f_3 of cell 8 as the most degraded RF that should be relocated from its OC λ_4. Supported by the QoT-tool, the algorithm computes the share of each impairment and identifies IMDs as the most penalizing noise $\mathcal{I}$. According to Table II, 4 rules can be exploited to mitigate IMDs. Once all OCs are ranked with respect to each rule $\mathcal{R}_\ell$, the aggregated rank is computed as in Equation 14 while the rank of OC λ_4 is set to 0. Showing the highest rank, OC λ_1 is selected for RF permutation with OC λ_4. Given the new RF-onto-OC mapping solution, GSB uses the QoT-tool to evaluate its capacity matrix ρ before computing its quality Ω.

IV. Simulations and Numerical Results

To evaluate the performance of the DBS algorithm, we consider a radio network composed of 20 cells of $500m$ radius and operating with the LTE radio system. Radio cells are

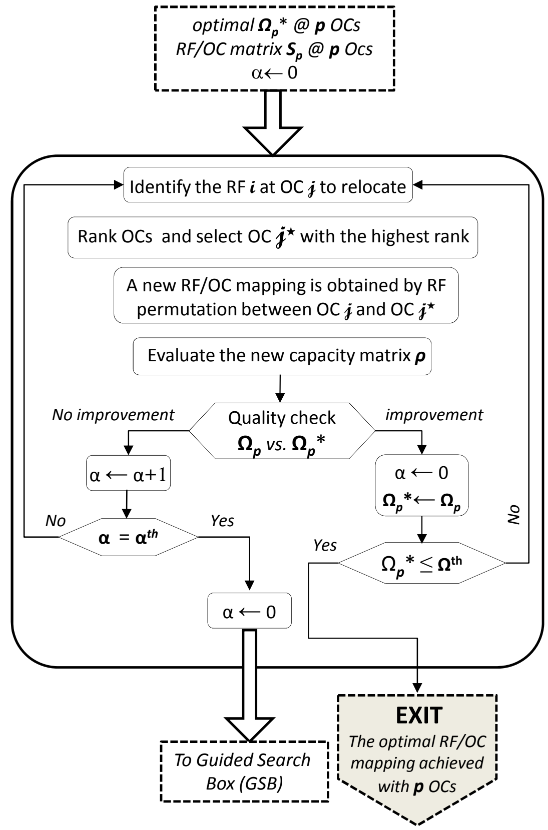

Fig. 8: Blind Search Box (BSB) flowchart.

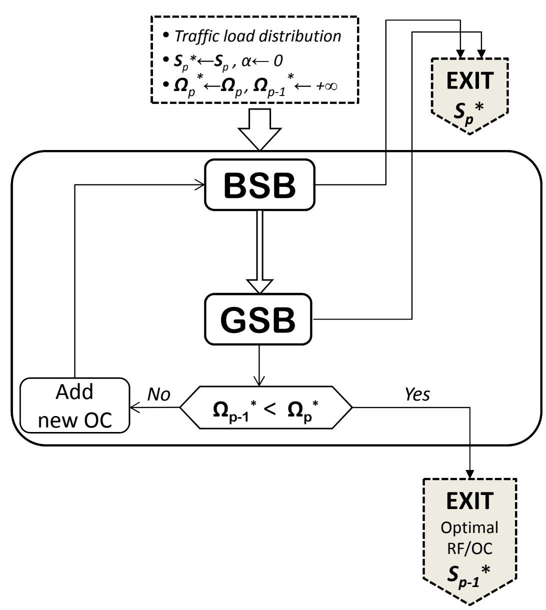

Fig. 9: DBS^{-} algorithm flowchart.

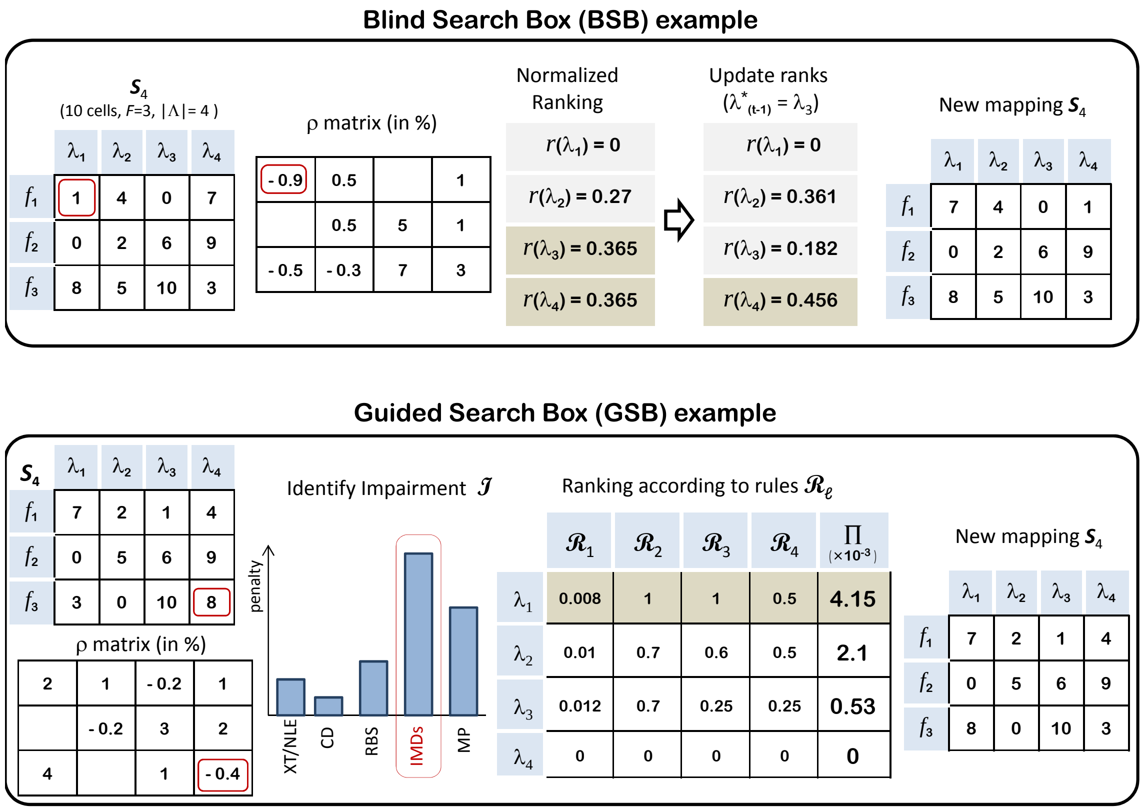

Fig. 11: Illustrating through an example the main steps of the BSB and GSB blocks.

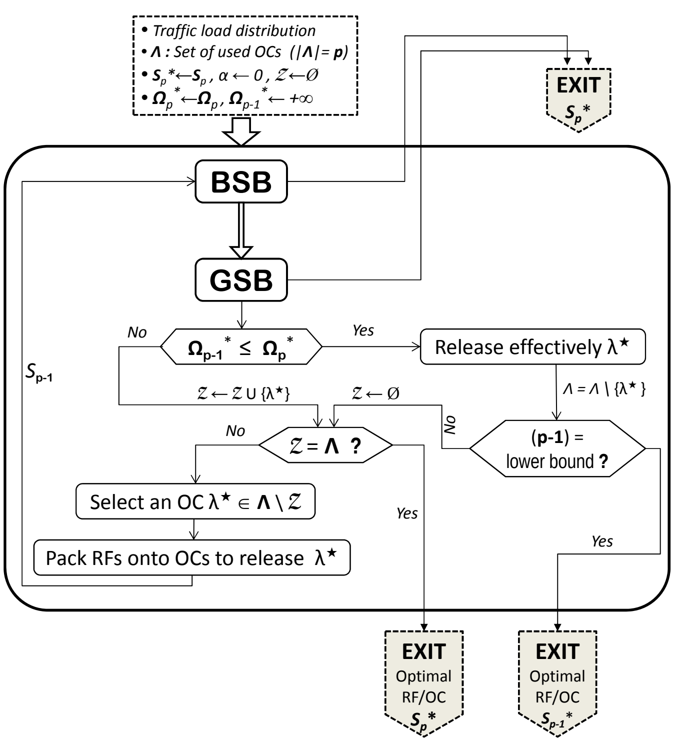

Fig. 10: DBS$^+$ algorithm flowchart.

backhauled via the GeRoFAN optical tree by selecting the splitting node at the center of the cellular network so that all RAUs are uniformly distributed around the splitting node. The radio spectrum pool is made of $F = 7$ RFs with 5 MHz each in the 2.5 GHz band. RFs are regularly reused among cells as illustrated in Figure 12.

The λ-pool is made of $W = 24$ OCs equally spaced of $1nm$ within the C-band. Users are located at half-way from the RAU's antenna. Mobile equipment transmit with a power of $+10dB$. Radio propagation including signal attenuation due to free-space propagation, shadowing and cellular radio interference is modeled as in [26]. Assuming voice service requiring 32 $kbps$ per call and considering the Shannon's capacity, the rejection ratio in each cell is calculated with respect to legacy cellular backhauling (i.e. RF demodulation and processing are carried out at the RAU).

The simulation scenario is initialized by considering that all cells are subject to the same load set to 50%. As a starting point, RFs are mapped onto the lower bound of required OCs (here equals to 3 according to the RF reuse pattern depicted in Figure 12). We select randomly 4 radio cells in the network to play the role of hot-spots. The load in hot-spots is increased by an increment of 5% over repetitive time periods. Such an increment can easily be tracked by the traffic load monitor. At each load increase, the CP runs DBS (in this case DBS^+) to investigate the optimal RF-onto-OC mapping solution able to provision the required capacity with the lowest number of OCs. To find the optimal RF-onto-OC mapping solution at a given time period, DBS starts its search from the optimal

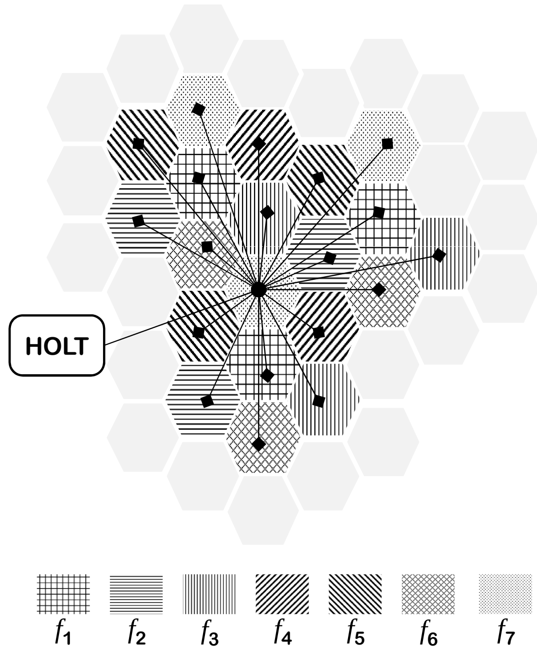

Fig. 12: Network configuration for simulation scenario.

TABLE III: Average rejection ratios, Ψ^* and required number of OCs $|\Lambda^\star|$ achieved by DBS$^+$ when 4 hot spot cells experience an increase of the traffic load. DBS ends with an incompressible excess capacity $\xi \simeq 27\%$.

	load (%)	rejection (%)	Ψ^* (%)	$\lvert\Lambda^\star\rvert$	DBS achieved by:
figure 13	50	0	133	3	no specific action required.
	55	0	127 ± 0.5	3	no specific action required.
	60	0	116 ± 0.5	3	RF/λ remapping.
	65	0	107 ± 0.5	3	RF/λ remapping.
figure 14	70	0	105 ± 0.7	4	RF/λ remapping. Adding a new OC.
	75	0	101 ± 1	4	RF/λ remapping.
	80	0	100.8 ± 1	5	RF/λ remapping. Adding a new OC.
	85	3 ± 0.5	96.7 ± 1.5	6	RFλ remapping. Adding a new OC.
figure 15	90	5 ± 0.5	92.3 ± 1.5	7	RF/λ remapping. Adding a new OC.
	95	9.5 ± 1	89 ± 2	7	RF/λ remapping.
	100	11.6 ± 1.8	86 ± 2	7	RF/λ remapping.

solution achieved at the previous time period. We run DBS with the following parameters: $\alpha^{th} = 25$ and $\Omega^{th} = 10^{-5}$.

Two metrics are used to track the performance of the DBS algorithm. We define Ψ as the ratio of the provisioned capacity to the requested capacity, averaged over all hot-spots. To highlight how the algorithm achieves the transfer of radio capacity to feed hot-spots with the required capacity, we define the excess capacity ξ ($\xi \geq 0$) as the the ratio of the gap between the offered and the required capacities normalized to the required capacity. ξ is averaged over all cells other than the designated hot spots.

Apart the value of Ψ^* achieved by the optimal RF-onto-OCs mapping solution at each load of the hot-spot cells, Table III shows the rejection ratio, the required number of OCs and specifies the main actions undertaken by the DBS algorithm to achieve the optimal solution. Since the 4 hot-spots are selected randomly among the 20 radio cells, results in Table III stand for the value averaged over $\binom{4}{20} = 4845$ possible scenarios and the standard deviation margin is also specified. Numerical results of Table III are reported to Figures 13, 14 and 15 illustrating the evolution of Ψ and ξ along iterations when the load at hot-spots increases from 50% to 65% (moderate load), then to 85% (high load) and finally to 100% (very high load) respectively.

Let's analyze the behavior of the DBS algorithm when the load increases. When hot-spots are subject to moderate load (i.e. up to 65%), the CP is able to provision the required capacity by optimizing the placement of RFs onto OCs. The needed capacity in hot-spots is filled at the detriment of the other cells (subject to lower load) as highlighted by the decrease of the excess capacity in Figure 13. Note that at 65% traffic load, an excess capacity of 7% can be derived at hot-spots, while up to 55% no specific action is need by the CP to satisfy the load apart reassigning uniformly the excess capacity among hot-spots.

However, when the hot-spot is subject to high load (c.f. Figure 14), it may be necessary to add new OCs when only a remapping of RF-onto-OCs is not sufficient to provision the required capacity. According to Table III, first optimal solutions leading to rejection are obtained when the load lies between 80% and 85%. Such a particular value of the load is called *critical load*. It is worth noting that when the load at hot-spots attains the critical load, the DBS backhauling solution cannot absorb completely the load. In that case, only providing a new RF is able to provision the capacity required to serve all calls. On Figure 14, we distinguish the two optimization approaches constituting the DBS algorithm. Under BSB, Ψ increases as a stair function with small amplitudes and large step iterations, while with GSB this stair function is characterized by large amplitudes and small steps. Thus, BSB and GSB correspond respectively to a disruptive and an incremental evolution of Ψ.

At very high loads, DBS is not able to provide the requested capacity as outlined by the values of rejection ratios and $\Psi^* < 100\%$. Figure 15 shows that for loads higher than 95%, providing a new OC is worthless while the excess capacity achieves a plateau (equal to $\simeq 27\%$) called the *incompressible capacity*. The *incompressible capacity* is the ultimate limit of ξ beyond which the rationale of DBS, consisting in feeding hot-spots with capacity drawn from the excess of the other cells, becomes ineffective.

Figure 16 illustrates the incompressible excess capacity (ξ) and the critical load computed by DBS according to the number of hot-spot cells in the network. Up to 12 hot-spots, an incompressible excess capacity ranges between 20% and 30% hosted in the other 8 under-loaded cells. Such an unused capacity could be exploited by the radio operator in applying promotional fees in under-loaded cells in order to exploit the system at its full capacity. Such an approach benefits to both mobile users and the radio operator.

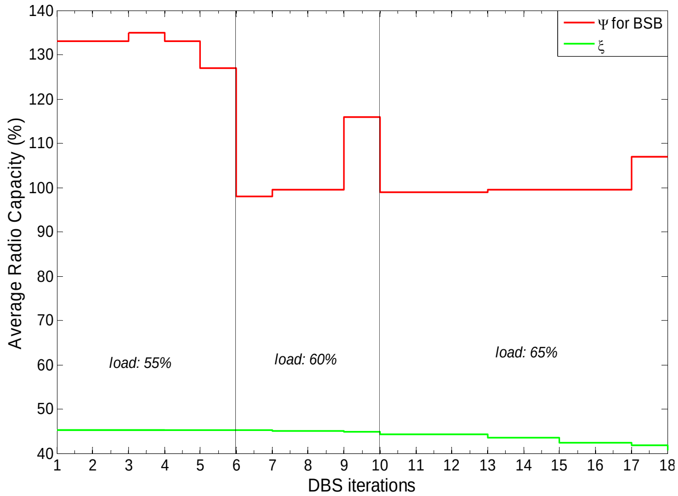

Fig. 13: Running DBS$^+$ as the load (inset figure) in the 4 hot spot cells increases from 50% to 65%.

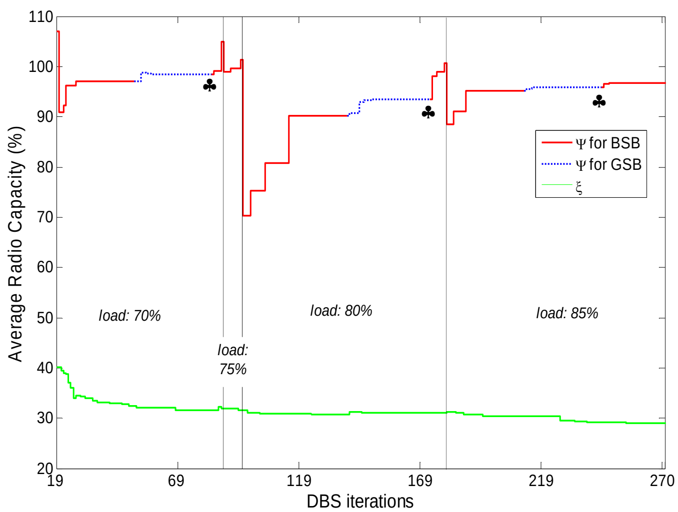

Fig. 14: Running DBS$^+$ as the load (inset figure) increases from 65% to 85%. ♣ denotes the adding of a new OC.

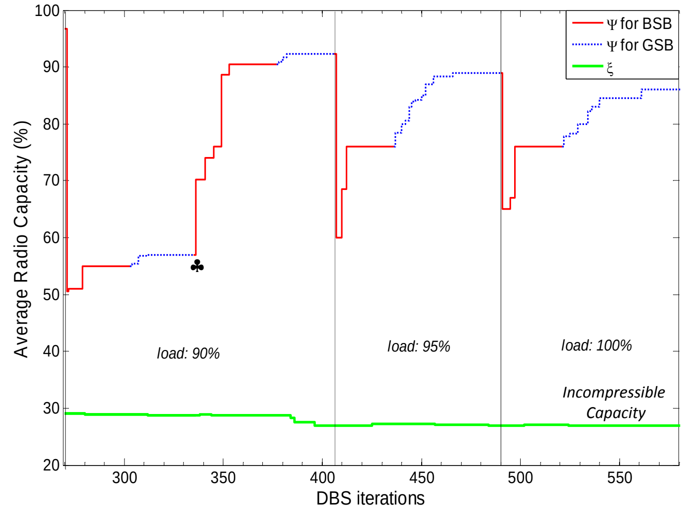

Fig. 15: Running DBS$^+$ as the load (inset figure) increases from 85% to 100%. ♣ denotes the adding of a new OC. Attained *Incompressible Capacity* $\simeq 27\%$.

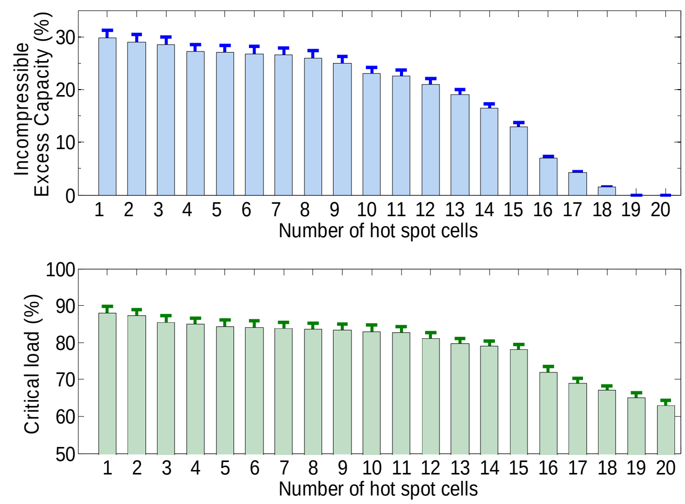

Fig. 16: Incompressible excess capacity and critical load *vs.* the number of hot spot cells in the cellular network.

Critical load *vs.* the number of hot-spot cells is also depicted in Figure 16. Let us consider an operator serving an urban area. This operator knows *a priori* the ratio of hot-spots in the considered area. From the critical load depicted in Figure 16, whatever the density of hot-spots up to 50%, the operator does not need additional RFs than the same RFs mentioned in Figure 12. If the hot-spot density is higher than 50% one notices that the probability the operator requests additional RFs from the regulator increases with the number of hot-spots. Since purchasing an additional RF is very expensive for an operator according to the current regulatory environment, this highlights the benefit of the DBS algorithm exploited by the GeRoFAN-CP.

V. Conclusion

The evolution of mobile backhauling is currently widely discussed between operators and equipment vendors. In this context, the GeRoFAN architecture and its control plane constitute a promising alternative enabling a high flexibility of radio resources allocation in 4G cellular networks. The GeRoFAN-CP relies on two key innovative aspects. We have proposed a QoT-tool enabling to quantify the impact of all physical layer impairments inherent to RoF transmission in PON access system. A decision support tool based on a set of rules has been proposed to mitigate the impact of these impairments on cellular capacity. The GeRoFAN-CP uses a Differentiated Backhauling Service (DBS) that adjusts dynamically the Shannon's capacity in each cell according to the traffic load by optimizing the RF-onto-OC mapping. The efficiency of the DBS approach has been demonstrated through numerical simulation scenario. By Unlike legacy backhauling systems, the GeRoFAN directly contributes to cellular capacity planning. The GeRoFAN-CP. Given the scarcity of RF resources and cost of radio licences, the GeRoFAN-CP enables to differ the need for additional RFs for the operators helping them leverage on significant cost savings. Since it is possible to assign optical channels to different operators and thanks to optical transparency, GeRoFAN can be viewed as an enabler for mobile backhauling mutualization. Such en environment necessitates an evolution of the regulatory context where the GeRoFAN infrastructure is managed by a third party (either a regional authority or a private independent backhaul operator).

Our coming studies will deal with the integration of business strategies in the DBS in order to facilitate radio resources mutualization between multiple operators to the benefit of both the GeRoFAN manager and radio operators.

References

[1] S. Chia, M. Gasparroni, P. Brick, *TheNext Challenge for cellular networks: backhaul*, IEEE Microwave Magazine, pp. 54-66, August 2009.

[2] O. Tipmongkolsilp, S. . Zaghloul, A. Jukan, *The evolution of Cellular Backhaul technologies: current issues and future trends*, IEEE Communications Surveys and Tutorials, pp. 97-113, Vol. 13, N.1, First Quarter 2011.

[3] S. Sesia, M. Baker and I. Toufik, *LTE: The UMTS Long Term Evolution: From Theory to Practice*, John Wiley and Sons Ltd., 2009.

[4] D. Wake, A. Nkansah and N. J. Gomes, *Radio-over-Fiber link design for Next-Generation Wireless systems*, IEEE Journal of Lightwave Technology, Vol. 28, N. 16, August 2010.

[5] A. Nirmalatha, P. A. Gamage, C. Lim, D; Novak and R. Waterhouse, *Digitized Radio-over-Fiber technologies for converged Optical Wireless Access Network*, IEEE Journal of Lightwave Technology, Vol. 28, N. 16, August 2010.

[6] M. A. ALi, G. Ellinas, H. Erkan, A. Hadjuantonis and R. Dorsinville, *On the vision of complete fixed-mobile convergence*, IEEE Journal of Lightwave Technology, Vol. 28, N. 16, August 2010.

[7] M. A. ALi, G. Ellinas, H. Erkan, A. Hadjuantonis and R. Dorsinville, *On the vision of complete fixed-mobile convergence*, IEEE Journal of Lightwave Technology, Vol. 28, N. 16, August 2010.

[8] Nokia Simens Networks Corporation White Paper, *Liquid Radio: Let traffic waves flow most efficiently*, url: www.nokiasimensnetworks.com, 2011.

[9] W. C. Babcock, *Intermodulation interference in radio systems*, Bell Systems Technical Journal, pp. 63-73, January 1953.

[10] J. Attard and J. Mitchell, *Optical network architectures for dynamic reconfiguration of full-duplex multi-wavelength radio-over-fiber*, IEEE Journal of Optical Networking, Vol. 5, N. 6, June 2006.

[11] M. Gagnaire and T. Youssef, *HOWRAN: an Hybrid Optical Wireless Radio Access Network for WiMAX antennas backhauling*, in Proceedings of IEEE/Accessnets, 2008.

[12] A. Haddad and M. Gagnaire, *Pareto Optimization for Radio-over-Fiber 4G Base Stations Backhauling*, To appear in proceedings of 15^{th} Int. Telecommunications Network Strategy and Planning Symposium, IEEE/Networks, October 2012.

[13] A. Haddad, M. Gagnaire and E. A. Doumith, *Impairment-Aware Control Plane for Next Generation Radio-over-Fiber Access Networks*, IEEE/Int. Conf. on the Network of the Future, pp. 92-96, November 2011.

[14] A. Haddad, E. A. Doumith and M. Gagnaire, *Impairment-Aware Radio-over-Fiber Control Plane for LTE Antenna Backhauling*, IEEE/Int. Conf. on Communications (ICC), pp. 2849-2854, June 2012.

[15] A. Haddad and M. Gagnaire, *Next Generation Access Systems Backhauling using Radio-over-Fiber: a Prospective Approach*, To appear in 2012 IEEE Photonics Society Summer Topical Meeting Series, July 2012.

[16] G. L. Li, C. K. Sun, S. A. Pappert, W. X. Chen and P. K. L. Yu, *Ultrahigh-speed traveling-wave electroabsorption modulator: design and analysis*, IEEE/ Transactions on Microwave Theory and Techniques, vol. 27, N. 7, pp. 1177-1183, July 1999.

[17] G.-W. Lee and S.-K. Han, *Linear-dual electroabsorption modulator for analog optical transmission*, Microwave and Optical Technology Letters, vol. 22, pp. 369-373, 1999.

[18] T. Niiho, M. Nakaso, K. Masuda, H. Sasai, K. Utsumi and M. Fuse, *Transmission performance of multichannel wireless LAN system based on Radio-over-Fiber techniques*, IEEE/ Transactions on Microwave Theory and Techniques, vol. 54, N. 2, pp. 980-989, February 2006.

[19] O. K. Tonguz and H. Jung, *Personal communications access networks using subcarrier multiplexed optical links*, IEEE/ Journal of Lightwave Technology, vol. 14, N. 6, pp. 1400-1409, June 1996.

[20] C. Desem, *Optical interference in subcarrier multiplexed systems with multiple optical carriers*, IEEE/ Journal on Selected Areas in Communications, vol. 8, N. 7, pp. 1290-1295, September 1990.

[21] P. Wan and J. Conradi, *Impact of double Rayleigh backscatter noise on digital and analog fiber systems*, IEEE/ Journal of Lightwave Technology, vol. 14, N. 3, pp. 288-297, March 1996.

[22] C. Sui *et al.*, *Impact of electroabsorption modulator integrated laser on MB-OFDM ultra-wideband signals over fiber systems*, IEEE/ Journal of Lightwave Technology, vol. 28, N. 24, pp. 3548-3555, December 2010.

[23] S. K. Narayankhedkar and R. K. Shevgaonkar, *Non-uniform fiber gratings in optical networks*, IEEE CLEO/ Pacific Rim'99, vol. 2, pp. 499-500, 1999.

[24] R. Hui, B. Zhu, R. Huang, C. T. Allen, K. R. Demarest and D. Richards, *Subcarrier multiplexing for high-speed optical transmission*, IEEE/ Journal of Lightwave Technology, vol. 20, N. 3, pp. 417-427, March 2002.

[25] S. D. Dods and R. S. Tucker, *A comparison of the homodyne crosstalk characteristics of optical add-drop multiplexers*, IEEE/ Journal of Lightwave Technology, vol. 19, N. 12, pp. 1829-1838, December 2001.

[26] P. Godlewski, M. Maqbool, M. Coupechoux and J.-M. Klif, *Analytical evaluation of various frequency reuse schemes in cellular OFDMA networks*, in Proceedings of the 3^{rd} Int. Conf. on Performance Evaluation Methodologies and Tools, pp. 32:1-32:10, 2008.

Dépôt légal : 2013 – 4ème trimestre
Imprimé à Télécom ParisTech – Paris
ISSN 0751-1337 ENST C (Paris) (France 1983-9999)

Télécom ParisTech

Institut Mines - Télécom - membre de ParisTech

46, rue Barrault - 75634 Paris Cedex 13 - Tél. + 33 (0)1 45 81 77 77 - www.telecom-paristech.frfr

Département INFRES

© Institut Mines - Télécom, Télécom ParisTech 2013